

Highly Active Heterogeneous Catalyst for Ethylene Dimerization Prepared by Selectively Doping Ni on the Surface of a Zeolitic Imidazolate Framework

Cailing Chen,[▲] Mohammed R. Alalouni,[▲] Xinglong Dong,[▲] Zhen Cao, Qingpeng Cheng, Lirong Zheng, Lingkun Meng, Chao Guan, Lingmei Liu, Edy Abou-Hamad, Jianjian Wang, Zhan Shi, Kuo-Wei Huang, Luigi Cavallo, and Yu Han*



Cite This: *J. Am. Chem. Soc.* 2021, 143, 7144–7153



Read Online

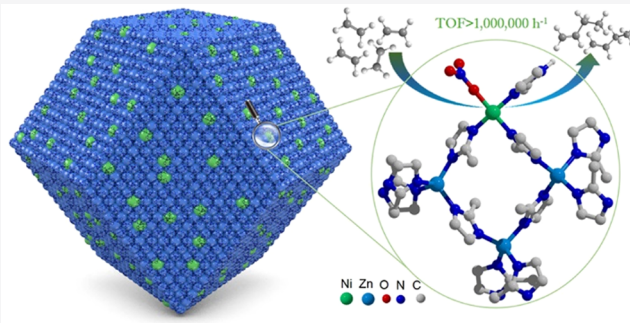
ACCESS |

Metrics & More

Article Recommendations

Supporting Information

ABSTRACT: The production of 1-butene by ethylene dimerization is an important chemical industrial process currently implemented using homogeneous catalysts. Here, we describe a highly active heterogeneous catalyst (Ni-ZIF-8) for ethylene dimerization, which consists of isolating Ni-active sites selectively located on the crystal surface of a zeolitic imidazolate framework. Ni-ZIF-8 can be easily prepared by a simple one-pot synthesis method in which site-specific anchoring of Ni is achieved spontaneously because of the incompatibility between the d⁸ electronic configuration of Ni²⁺ and the three-dimensional framework of ZIF-8. The full exposure and square-planar coordination of the Ni sites accounts for the high catalytic activity of Ni-ZIF-8. It exhibits an average ethylene turnover frequency greater than 1 000 000 h⁻¹ (1-butene selectivity >85%) at 35 °C and 50 bar, far exceeding the activities of previously reported heterogeneous catalysts and many homogeneous catalysts under similar conditions. Moreover, compared to molecular Ni complexes used as homogeneous catalysts for ethylene dimerization, Ni-ZIF-8 has significantly higher stability and shows constant activity during 4 h of continuous reaction. Isotopic labeling experiments indicate that ethylene dimerization over Ni-ZIF-8 follows the Cossee-Arlman mechanism, and detailed characterizations combined with density functional theory calculations rationalize this observed high activity.



INTRODUCTION

Linear α -olefins are of great importance to the chemical industry. 1-Butene is the most in-demand linear α -olefin, which is widely used to produce unique polyethylene varieties such as linear low-density and high-density polyethylene.¹ As a dedicated technology, ethylene dimerization has found significant success in the global production market of 1-butene, largely because of its lower operating cost compared to other technologies based on refinery fractionation, steam cracking, and ethylene oligomerization. Currently, the commercial ethylene dimerization processes use homogeneous catalysts composed of transition-metal (e.g., Ni, Ti, and Ta) complexes.^{2–5} Despite their high activity and selectivity, these homogeneous molecular catalysts have a short lifetime and are difficult to separate.

The high activity of homogeneous molecular catalysts is partly due to their easy accessibility for reactant molecules and, more importantly, to the well-defined coordination environment provided by the ligands for the metal center. Previous studies have extensively investigated the important influence of the type of ligands and their configuration around

the metal center on the catalytic activity.^{6–8} Because it is difficult to introduce ligands with molecular precision into the support materials traditionally used for heterogeneous catalysis, the development of heterogeneous catalysts for ethylene dimerization has not been very successful. Various metals supported on oxides, zeolites, and mesoporous silica materials have been tested;^{9–14} however, their activities, in terms of the number of ethylenes consumed per catalytic active site per unit time (usually referred to as turnover frequency (TOF)), are generally several orders of magnitude lower than the activities of the benchmark homogeneous catalysts under similar reaction conditions.¹⁵ The development of highly active, selective, and stable heterogeneous

Received: February 28, 2021

Published: April 28, 2021



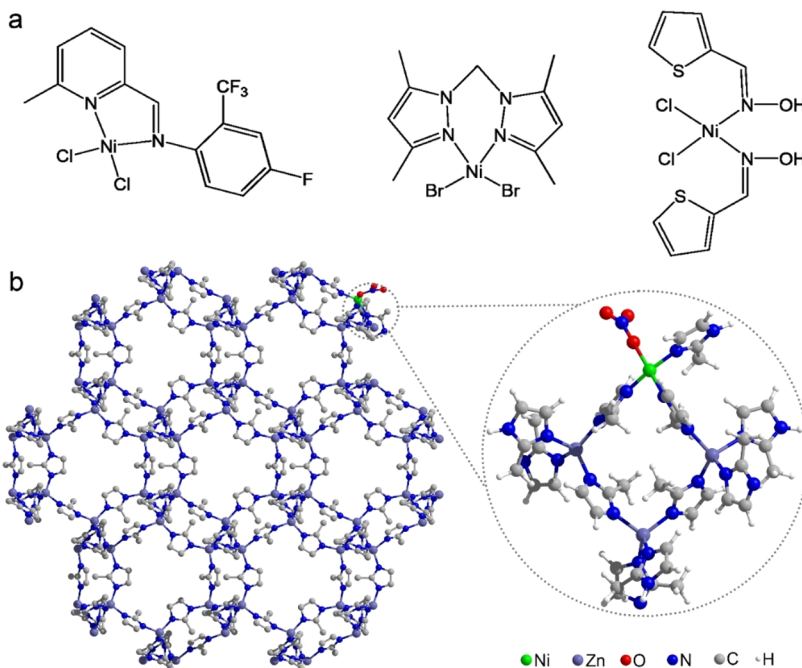


Figure 1. (a) Representative four-coordinated, imine-chelated Ni complexes used as homogeneous catalysts for ethylene dimerization. (b) Coordination structure of the Ni center on the crystal surface of Ni-ZIF-8 proposed based on characterizations and optimized by DFT calculations. In the structural model on the left, hydrogen atoms are omitted for clarity.

catalysts for ethylene dimerization remains a significant challenge.

Metal–organic frameworks (MOFs) composed of metal centers and organic coordinating ligands are analogues of molecular metal–organic compounds in solid materials. Therefore, MOFs represent a conceptually new platform for heterogeneous catalysis, allowing easy translation of the established structure–activity relationships from homogeneous catalytic systems. MOF-based catalysts for ethylene dimerization have been reported previously, in which the active sites are coordinately unsaturated metal sites or are generated by immobilizing molecular metal complexes on the MOF frameworks.^{16–30} These catalysts have been tested in liquid-phase batch reactions^{16–24} and gas-phase fixed-bed reactions,^{27–30} but the latter usually gives much lower conversions. Dinca et al. reported a series of interesting works in which they exchanged Zn²⁺ in MOF MFU-4l with Ni²⁺ to create isolating active sites that are structurally homologous to molecular [Tp^{Mes}Ni]⁺ complexes.^{17,18,31,32} The obtained Ni-MFU-4l is one of the most active and stable heterogeneous catalysts for ethylene dimerization reported to date, showing an average (1 h) TOF of 41 500 h⁻¹ at 25 °C and 50 bar in a batch reaction.¹⁷

In this study, we design a new MOF-based catalyst based on the following considerations. We note that many reported homogeneous ethylene dimerization catalysts with high activity have a common structural moiety, that is, Ni²⁺ coordinated with two imine groups and two other ligands (halogens in most cases), where the two imine groups can be provided by one bidentate ligand (e.g., pyridinylimine and diimine) or by two monodentate imine ligands (see Figure 1).^{33–36} To mimic the chelation of Ni by diimine in such molecular complexes, we doped Ni into a Zn-based zeolitic imidazolate framework (ZIF-8). Because the d⁸ electron configuration of Ni²⁺ favors a square-planar coordination that is not compatible with the three-dimensional (3D) MOF

framework, Ni cannot replace Zn at the tetrahedral sites in this framework. Thus, Ni can reside only on the ZIF-8 crystal surface where the preferred square-planar coordination structure is allowed. The presence of active Ni sites on the crystal surface is advantageous because it not only eliminates the mass-transport limitation imposed by the microporous structure but also, more importantly, provides sufficient freedom to the Ni centers to adopt an optimal coordination state and expose more vacant sites for ethylene coordination, resulting in excellent catalytic activity. In addition, unlike previous works that required postsynthesis modification to introduce active sites onto the MOF, our design realizes site-selective doping of Ni through one-pot synthesis by taking advantage of the incompatibility between Ni and the ZIF-8 framework.

Our Ni-doped ZIF-8 (denoted as Ni-ZIF-8) catalysts with different Ni loadings were examined for ethylene dimerization under different reaction conditions. At 35 °C and 50 bar ethylene pressure, the Ni-ZIF-8 shows excellent activity with an initial TOF of 1 116 000 h⁻¹ (the average result of a 10 min reaction), far exceeding the activities of existing heterogeneous catalysts and even many homogeneous catalysts. Compared to homogeneous catalysts that rapidly deactivate within tens of minutes, Ni-ZIF-8 exhibits stable activity and selectivity for C₄ products in 4 h of reaction, resulting in a substantially higher total conversion capacity.

RESULTS AND DISCUSSION

Preparation and Characterizations of Ni-ZIF-8. Ni-ZIF-8 can be easily synthesized by mixing the metal salts, Ni(NO₃)₂ and Zn(NO₃)₂, with the organic ligand 2-methylimidazole in methanol at room temperature and stirring for 10 h (see the Supporting Information for details). In this study, we prepared four Ni-ZIF-8 samples with different Ni loadings by varying the molar ratio of Ni to the total amount

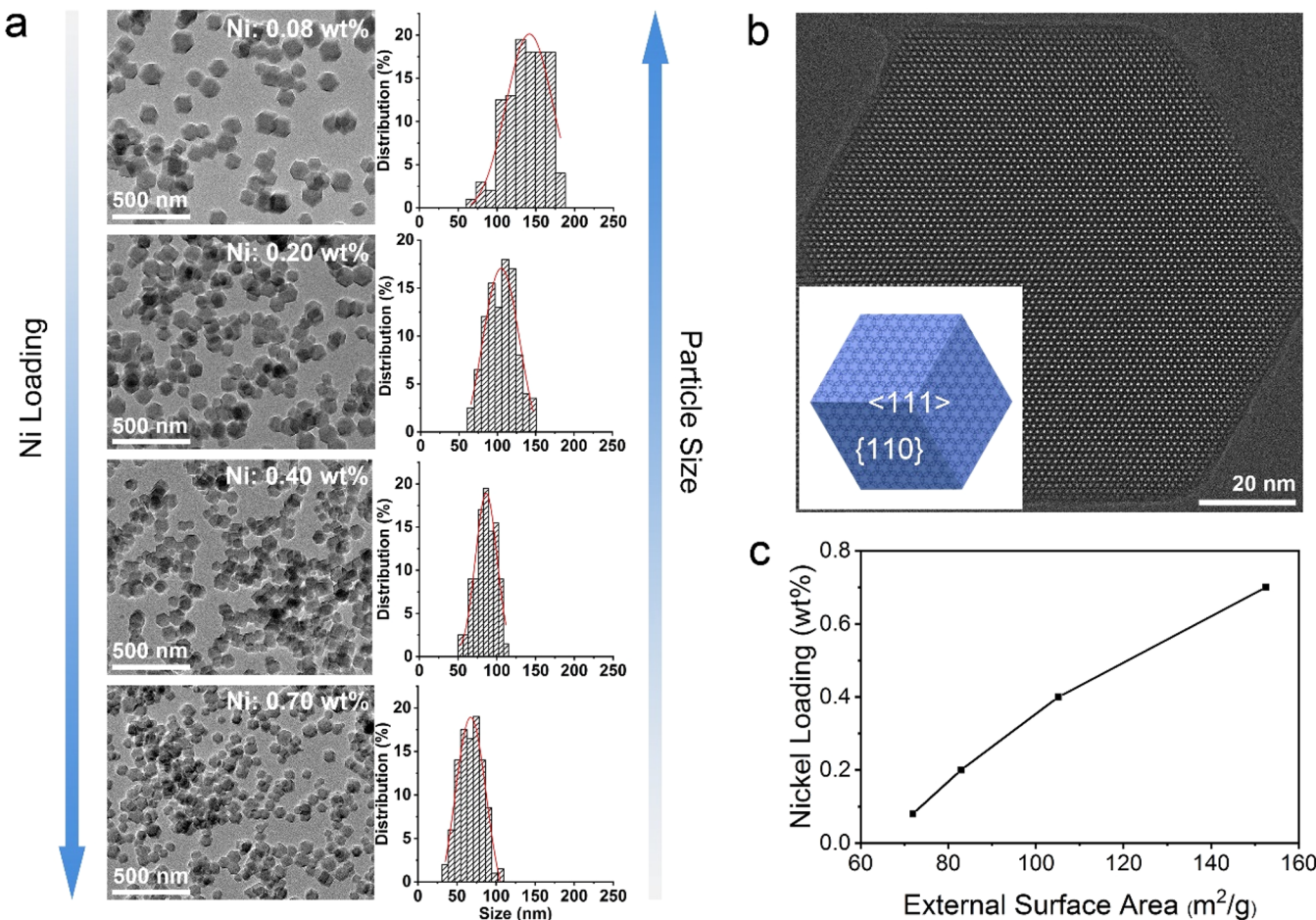


Figure 2. (a) Low-magnification TEM images of Ni-ZIF-8 samples with different nickel loadings: 0.08, 0.20, 0.40, and 0.70 wt %. The crystal size distributions are statistical results obtained by measuring the sizes of 100 discrete crystals from multiple images. (b) High-resolution TEM image of Ni-ZIF-8 with Ni loading of 0.70 wt %, acquired along the $\langle 111 \rangle$ zone axis. Inset is a schematic illustration of a rhombic dodecahedral crystal oriented along the $\langle 111 \rangle$ direction and exposing 12 $\{110\}$ facets. (c) Plot of the nickel loading versus the external surface area of Ni-ZIF-8, showing a positive linear correlation.

of metals (Ni + Zn) in the synthetic precursor (15%, 30%, 45%, and 60%) while keeping the total amount of metals and the concentration of 2-methylimidazole unchanged.

The four Ni-ZIF-8 samples all showed characteristic powder X-ray diffraction patterns of ZIF-8 (Figure S1) and were all purple in color, unlike the pure white undoped ZIF-8 (Figure S2). We observed two notable phenomena. First, despite the large amount of nickel added to the synthetic precursor, the nickel content in the four Ni-ZIF-8 samples was very limited: 0.08, 0.20, 0.40, and 0.70 wt %. Second, the crystal size of Ni-ZIF-8 decreased monotonically with the increase of Ni content; the average crystal sizes of the four samples were 135, 105, 85, and 67 nm, as determined from the low-magnification TEM images (Figure 2a). Undoped ZIF-8 synthesized under the same conditions had an average crystal size of 165 nm (Figure S2). We derived the external surface areas of the four Ni-ZIF-8 samples from their N₂ adsorption isotherms using the *t*-plot method and found that Ni loading had a positive linear correlation with the external surface area of the sample (Figure 2c, Figure S3). In a separate experiment, we synthesized large Ni-ZIF-8 crystals (~320 nm, Figure S4) by decreasing the concentration of 2-methylimidazole by fourfold. The obtained sample contained only trace amounts of Ni (<0.02 wt %) despite the high Ni/Zn ratio (3:2) in the synthetic precursor, further confirming the direct correlation

between the external surface area (i.e., the crystal size) and the Ni loading. These results taken together indicate that the presence of Ni in the synthetic system suppressed the growth of ZIF-8 crystals, while the doped Ni atoms were located only on the crystal surface. This finding agrees with our hypothesis that divalent nickel tends to adopt a square-planar coordination that is not compatible with the tetrahedral framework of ZIF-8, thereby leading to site-selective doping of Ni.

While the four Ni-ZIF-8 samples all showed high catalytic activity for ethylene dimerization (see Table 1), we selected the sample with the highest Ni loading (0.70 wt %) for more detailed characterization. The TEM images revealed that although the crystal sizes were small, Ni-ZIF-8 still had the characteristic rhombohedral dodecahedron morphology of conventional ZIF-8. The high-resolution TEM image acquired along the $\langle 111 \rangle$ zone axis confirmed the highly ordered crystal structure and well-defined crystal shape of Ni-ZIF-8 (Figure 2b). Since rhombohedral dodecahedron crystals expose only $\{110\}$ facets, the number of metal atoms located on the crystal surface can be approximately calculated based on the $\{110\}$ surface structure of ZIF-8 (2.5 metal atoms/nm²) and the determined external surface area (150 m²/g). Combining the calculation result (3.75×10^{20} metal atoms/g of ZIF-8) with the Ni loading (0.70 wt %), the Ni/(Zn+Ni) ratio on the

Table 1. Catalytic Ethylene Dimerization Using Ni-ZIF-8^a

entry	catalyst ^b	TOF ^c (h ⁻¹)	selectivity ^d	MAO conc. (mol/L)	MAO equiv ^e	pressure (bar)	temperature (°C)
1	ZIF-8	0	0	0.075		30	35
2	Ni-ZIF-8 (0.70 wt %)	0	0	0	0	30	35
3	Ni-ZIF-8 (0.08 wt %)	288 000	C4 = 93.8% (1-C4 = 94.4%)	0.075	15500	30	35
4	Ni-ZIF-8 (0.20 wt %)	274 000	C4 = 95.3% (1-C4 = 93.1%)	0.075	4640	30	35
5	Ni-ZIF-8 (0.40 wt %)	281 000	C4 = 95.9% (1-C4 = 89.3%)	0.075	2320	30	35
6	Ni-ZIF-8 (0.70 wt %)	297 000	C4 = 94.8% (1-C4 = 85.5%)	0.075	1320	30	35
7	Ni-ZIF-8 (0.70 wt %)	61 000	C4 = 96.7% (1-C4 = 92.7%)	0.0375	660	30	35
8	Ni-ZIF-8 (0.70 wt %)	570 000	C4 = 91.0% (1-C4 = 72.0%)	0.150	2650	30	35
9	Ni-ZIF-8 (0.70 wt %)	499 000	C4 = 91.4% (1-C4 = 75.0%)	0.225	4260	30	35
10	Ni-ZIF-8 (0.70 wt %, 30 mg)	246 000	C4 = 93.3% (1-C4 = 80.9%)	0.075	660	30	35
11	Ni-ZIF-8 (0.70 wt %, 5 mg)	291 000	C4 = 95.9% (1-C4 = 89.7%)	0.075	3400	30	35
12	Ni-ZIF-8 (0.70 wt %, 1 mg)	296 000	C4 = 97.1% (1-C4 = 93.2%)	0.075	19900	30	35
13	Ni-ZIF-8 (0.70 wt %)	44 100	C4 = 95.1% (1-C4 = 85.1%)	0.075	1320	10	35
14	Ni-ZIF-8 (0.70 wt %)	122 000	C4 = 95.3% (1-C4 = 85.3%)	0.075	1320	20	35
15	Ni-ZIF-8 (0.70 wt %)	467 000	C4 = 95.6% (1-C4 = 89.7%)	0.075	1320	50	35
16	Ni-ZIF-8 (0.70 wt %)	32 800	C4 = 97.9% (1-C4 = 97.9%)	0.075	1320	30	0
17	Ni-ZIF-8 (0.70 wt %)	323 000	C4 = 92.9% (1-C4 = 79.7%)	0.075	1320	30	50
18	Ni-ZIF-8 (0.70 wt %)	1 079 000	C4 = 90.8% (1-C4 = 74.5%)	0.15	2650	50	35
19	Ni-ZIF-8 (0.40 wt %)	1 116 000	C4 = 97.0% (1-C4 = 87.7%)	0.15	4640	50	35
20	Ni-ZIF-8@ZIF-8	43 300	C4 = 93.6% (1-C4 = 95.0%)	0.075	2650	30	35

^aReactions were conducted in a 75 mL Parr autoclave reactor; solvent, 20 mL of toluene; reaction time, 10 min. ^bThe amount of catalyst is 15 mg unless otherwise specified. ^cmol of ethylene/mol of Ni/h; average of the 10 min reaction. ^dThe 1-C₄ selectivity shown in the parentheses refers to the percentage of 1-butene in the C₄ products. ^eThe mole ratio of aluminum in MAO to nickel in the catalyst.

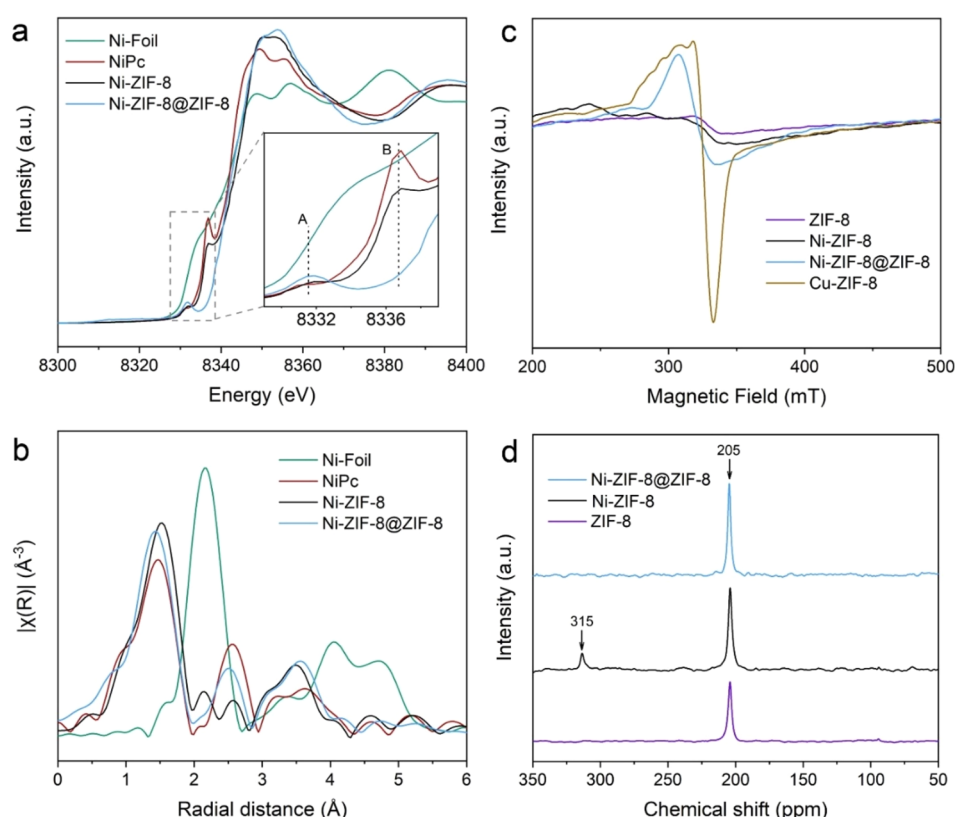


Figure 3. (a) Ni K-edge X-ray absorption near-edge structure (XANES) spectra and (b) Ni K-edge Fourier transformed extended X-ray absorption fine structure (EXAFS) spectra in the R space of Ni-Foil, NiPc, Ni-ZIF-8, and Ni-ZIF-8@ZIF-8. (c) EPR spectra and (d) ¹⁵N CP-MAS solid-state NMR spectra of ZIF-8, Ni-ZIF-8, and Ni-ZIF-8@ZIF-8. In (c), the spectrum of Cu-ZIF-8 is presented as a reference. The Ni-ZIF-8 sample used in these characterizations has a Ni loading of 0.70 wt %.

crystal surface was about 1:5. Energy-dispersive X-ray spectroscopy showed weak signals of Ni uniformly distributed

throughout the entire crystal (Figure S5). These results taken together indicate that the Ni atoms in Ni-ZIF-8 (0.70 wt %)

are isolated on the crystal surfaces as “single sites” at a density of 0.5 Ni atoms/nm². In the same way, the Ni site densities on the other three samples were calculated to be 0.41/nm² for Ni-ZIF-8 (0.40 wt %), 0.26/nm² for Ni-ZIF-8 (0.20 wt %), and 0.12/nm² for Ni-ZIF-8 (0.08 wt %), respectively (Table S1).

We conducted X-ray absorption spectroscopy (XAS) to probe the valence state and local structure of the Ni in Ni-ZIF-8, using Ni foil and nickel phthalocyanine (NiPc) as standard materials. Figure 3a shows the Ni K-edge X-ray-absorption near-edge structure (XANES) spectra of the various samples. The absorption edge of Ni-ZIF-8 appeared at a higher energy than that of the Ni foil and was very close to the absorption edge of NiPc, indicating a valence state of Ni²⁺.^{37,38} In addition, Ni-ZIF-8 had similar pre-edge features to NiPc, including a low-intensity peak at ~8332 eV (labeled as “A”) and an intense peak at ~8337 eV (labeled as “B”) (see Figure 3a, inset), which corresponded to the dipole-forbidden 1s → 3d transition and the 1s → 4p_z transition, respectively. Studies have considered these fine structure features of NiPc to be characteristic of Ni in a square-planar coordination configuration.³⁹ The resemblance of the XANES spectra of Ni-ZIF-8 and NiPc indicated that the Ni atoms in Ni-ZIF-8 were also square-planar-coordinated. Compared to NiPc, the B peak of Ni-ZIF-8 was less obvious, which implies that the coordination environment of Ni was not perfectly centrosymmetric and deviated from the ideal square-planar geometry.³⁷ Figure 3b presents the Fourier-transformed (FT) *k*³-weighted extended X-ray absorption fine structure (EXAFS) spectra. Ni-ZIF-8 and NiPc both showed a primary peak located at ~1.53 Å, which corresponded to the first coordination shell of Ni–N/O. We observed no Ni–Ni scattering path (~2.17 Å), confirming that the Ni was atomically dispersed in Ni-ZIF-8.

Ni-ZIF-8 had an electron paramagnetic resonance (EPR) spectrum similar to that of ZIF-8, showing no signals related to metal-centered unpaired electrons (Figure 3c). This result further confirmed that the Ni²⁺ in Ni-ZIF-8 adopted a square-planar coordination geometry because a tetrahedral-coordination geometry would otherwise lead to unpaired electrons and generate EPR signals. The fact that Cu-doped ZIF-8 showed a strong EPR signal proves the reliability of the EPR measurement (Figure 3c).

The square-planar coordination configuration of Ni²⁺ required no more than two ligands from the crystal framework (2-methylimidazole), which means that there were two or more nonframework free ligands. Interestingly, the ¹⁵N CP-MAS solid-state nuclear magnetic resonance (NMR) spectroscopy indicated an obvious difference between ZIF-8 and Ni-ZIF-8 (Figure 3d): both samples had a primary peak at 205 ppm arising from the 2-methylimidazole linker,⁴⁰ but Ni-ZIF-8 showed an additional peak at 315 ppm, which was assigned to the NO₃⁻ groups according to the ¹⁵N NMR spectra of nitrates (see Figure S6). This result suggests that NO₃⁻ was present on Ni-ZIF-8 as a surface ligand through specific interaction with Ni²⁺, but not on ZIF-8. On the basis of the synthetic conditions, we speculate that each Ni²⁺ cation on the crystal surface of Ni-ZIF-8 was four-coordinated by two 2-methylimidazole ligands from the crystal framework, one NO₃⁻ and one dangling 2-methyleimidazole, and we constructed a corresponding prototypical model. The optimized model presented a slightly deformed square-planar structure (see Table S2 for bond lengths and angles), even if

we forced the initial structure into a tetrahedral shape, which was consistent with the XAS and EPR characterizations.

To deepen our understanding of Ni-ZIF-8, we prepared a control sample. Specifically, we used as-synthesized Ni-ZIF-8 crystals as “seeds” to grow a shell of pure ZIF-8 on their surfaces. During the seeded growth process, the average crystal size increased from 67 to 90 nm (Figure S7), and the Ni loading decreased from 0.70 to 0.35 wt %. The obtained sample was denoted as Ni-ZIF-8@ZIF-8. Interestingly, unlike Ni-ZIF-8, Ni-ZIF-8@ZIF-8 did not have the characteristic peak at ~8337 eV (peak B) in the Ni K-edge XANES spectrum, which implies a transition from a square-planar to a tetrahedral coordination due to the coating of the ZIF-8 shell (Figure 3a). Meanwhile, the peak amplitude of the first coordination shell of Ni became higher after the seeded growth (Figure 3b), indicating that the local structural order was improved. Ni-ZIF-8@ZIF-8 showed a distinct EPR signal with a calculated *g* value of 2.1 (Figure 3c), consistent with other tetrahedrally coordinated Ni²⁺ reported in the literature.⁴¹ In addition, ¹⁵N CP-MAS NMR indicated that Ni-ZIF-8@ZIF-8 did not contain NO₃⁻ surface ligands (Figure 3d), which confirmed the specific correspondence between NO₃⁻ and surface Ni²⁺ and the successful growth of a Ni-free shell. These characterizations taken together demonstrate that although Ni atoms only resided on the crystal surfaces by one-pot, direct synthesis of Ni-ZIF-8, these surface-bonded Ni atoms were forced to change their coordination during the secondary growth process to enter the 3D ZIF-8 framework and were eventually encapsulated within the MOF crystals (located at the core/shell interface). Furthermore, the characterization results of Ni-ZIF-8@ZIF-8, in turn, corroborate our above conclusions on Ni-ZIF-8.

Catalytic Properties of Ni-ZIF-8 for Ethylene Dimerization. We conducted ethylene dimerization in the liquid phase using a batch reactor. Our standard reaction conditions for catalyst evaluation were as follows: 15 mg of Ni-ZIF-8 catalyst, 20 mL of dried toluene, and 1 mL of toluene solution of methylaluminoxane (MAO; 10 wt %) as the cocatalysts were loaded into a Parr autoclave reactor (75 mL), reacting for 10 min under 30 bar of ethylene at 35 °C. Pure ZIF-8 was inactive for this reaction (entry 1 in Table 1, Figure S8). In contrast, Ni-ZIF-8 was highly active. Specifically, the sample with 0.70 wt % Ni loading showed a TOF of 297 000 h⁻¹ (mol of ethylene/mol of Ni; average of the 10 min reaction), and the product contained 94.8% butenes (85.5% 1-butene) and 5.2% hexenes, without higher oligomers (entry 6 in Table 1, Figure S9). Despite the different crystal sizes, the other three Ni-ZIF-8 samples showed similar activities and selectivities (Table 1, entries 3–5) to the sample with 0.70 wt % Ni loading, indicating that mass transport had little effect on the catalytic properties of Ni-ZIF-8. These findings are inline with our design of catalyst in which the active Ni sites are located only on the crystal surface of these catalysts.

We investigated the effects of the amount of MAO, ethylene pressure, and reaction temperature on the performance of Ni-ZIF-8. The results show that MAO is indispensable for this reaction (Table 1, entry 2) and that the catalytic activity increased with the increase of MAO concentration and plateaued when the MAO concentration reached 0.15 M (Table 1, entries 7–9). When the amount of catalyst was changed and the MAO concentration was kept constant, the TOF value did not change significantly (Table 1, entries 10–12), indicating that the activity was influenced by the

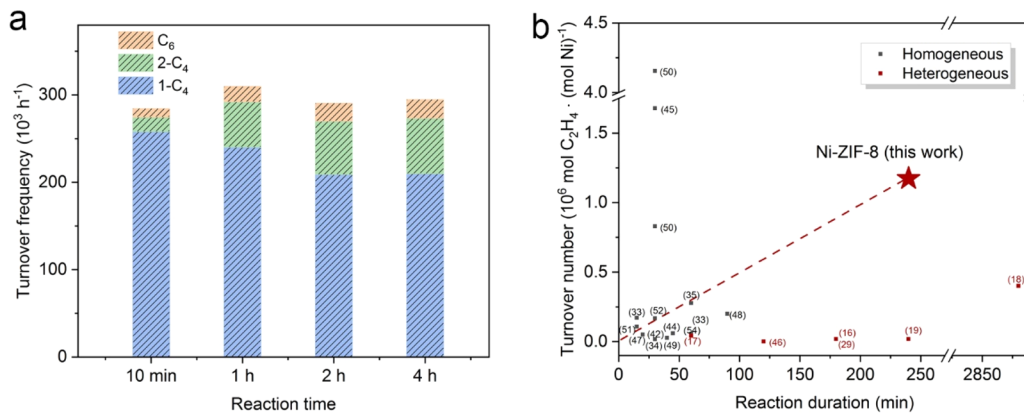


Figure 4. (a) Averaged TOFs and product distributions of ethylene dimerization on Ni-ZIF-8 at different reaction times. (b) Comparison of Ni-ZIF-8 with selected Ni-based homogeneous and heterogeneous catalysts. Turnover numbers are cited from the literature or calculated from the reported reaction duration and averaged TOFs. Note that, for many homogeneous systems, the catalyst was tested only in a short time without a specified lifetime determined; therefore, their turnover numbers shown here were achieved within the reaction time tested, not before the catalyst was completely deactivated. References are given for only a portion of the data points because of the limited space. Complete reference information is provided in Table S3.

concentration of MAO rather than the MAO/Ni ratio. This finding is also consistent with the observation that Ni-ZIF-8 catalysts with different nickel loadings exhibited the same level of activity at the same MAO concentration (Table 1, entries 3–6). Lower temperature and higher pressure are thermodynamically favorable for ethylene dimerization. Furthermore, despite the fast kinetics, a high reaction temperature causes the solubility of ethylene to decrease and promotes side reactions such as isomerization and chain growth. Therefore, ethylene dimerization is usually conducted at moderate temperatures (0–60 °C) and relatively high pressures (1–50 bar). We investigated the performance of Ni-ZIF-8 within these commonly used reaction temperature and pressure ranges (Table 1, entries 13–17). The TOF of Ni-ZIF-8 linearly increased with the increase in ethylene pressure in the range of 10–50 bar, indicating a first-order kinetics behavior (Figure S10). Under the conditions of 0.15 M MAO, 35 °C, and 50 bar, the Ni-ZIF-8 catalysts showed TOF values >1 000 000 h⁻¹ and C₄ selectivity up to 90% (Table 1, entries 18 and 19).

The high activity of Ni-ZIF-8 resulted in the quick accumulation of products in the reaction vessel as the reaction proceeded, which made it unsafe to run the reaction for too long. To evaluate the long-term stability of Ni-ZIF-8, we reduced the amount of catalyst to 1 mg (^{1/15} of the standard usage) to reduce the productivity of the system. As illustrated in Figure 4a, the catalyst showed nearly constant TOF values within 4 h, while the selectivity of 1-butene gradually decreased with the prolonged reaction time because of the isomerization of 1-butene to 2-butene (Figure S11).¹⁷ The combination of high activity and long-term durability gave Ni-ZIF-8 an excellent conversion capacity. We compared Ni-ZIF-8 with a number of reported Ni-based homogeneous and heterogeneous catalysts for ethylene dimerization by plotting the turnover number in one reaction versus the reaction duration (Figure 4b).^{16–19,29,33–35,42–54} In this plot, all data points use a unified unit (mol of ethylene/mol of Ni), and the slope of the line from the origin to each point represents the average TOF value of that catalyst. The specific reaction conditions of these data points are listed in Table S3. Although it is not appropriate to compare the absolute TOF values of different systems because the TOF values depend on

the reaction conditions, Figure 4b clearly illustrates the general characteristics of the homogeneous and heterogeneous catalysts; that is, homogeneous catalysts are active but easy to deactivate (usually tested for only 10–60 min in the literature); in comparison, heterogeneous catalysts are more durable but inherently less active. Figure 4b also indicates that Ni-ZIF-8 has the highest activity among all heterogeneous catalysts reported for ethylene dimerization, even surpassing many homogeneous catalysts, while also having excellent stability. Note that, for safety reasons, we stopped the reaction on Ni-ZIF-8 after 4 h when it remained highly active (Figure 4a). Nevertheless, the deduced turnover number of Ni-ZIF-8 is higher than that of all reference catalysts, except for two superactive homogeneous catalysts (Figure 4b).^{45,50}

After the reaction, we collected the used Ni-ZIF-8 catalyst by centrifugation for characterizations. TEM and STEM showed that Ni-ZIF-8 crystals maintained their original size and shape, but they had gel-like impurities attached. Energy-dispersive X-ray spectroscopy confirmed that Ni remained in the catalyst and revealed that the impurities were composed of Al (Figure S12). The gel-like Al species was derived from the cocatalyst MAO, which can produce aluminum (hydro)oxides and release a large amount of heat when in contact with moisture. Powder XRD indicated that the used Ni-ZIF-8 catalyst maintained the crystal structure but the crystallinity was reduced (Figure S12). The partial degradation of the crystal structure of Ni-ZIF-8 may have occurred during the XRD measurement when the residual MAO on the crystal surface reacted exothermically with air. ICP-OES analysis showed that compared to the fresh catalyst, the used catalyst had lower contents of Ni and Zn, but the Ni/Zn ratio was almost the same (Table S4). The reason for the lower Ni and Zn contents is the presence of additional Al species in the used catalyst, while the nearly constant Ni/Zn ratio proves that there is no Ni leaching or decomposition of catalyst during the reaction (considering that Ni is located only on the crystal surface, if Ni leaching or decomposition of the catalyst occurs, Ni/Zn will decrease). On the other hand, no nickel or zinc was detected in the supernatant collected from the reactor after the reaction. In addition, in a control experiment, we treated Ni-ZIF-8 with MAO in a toluene solution for 1 h and confirmed that the resulting supernatant is inactive for

ethylene dimerization (see Figure S13). All these results taken together rule out the possibility that the high activity came from a dissolved molecular Ni complex.

Reaction Mechanism of Ethylene Dimerization on Ni-ZIF-8. Two mechanisms have been proposed for catalytic ethylene dimerization in the literature. As illustrated in Figure 5a, the metallacyclic mechanism involves two ethylenes

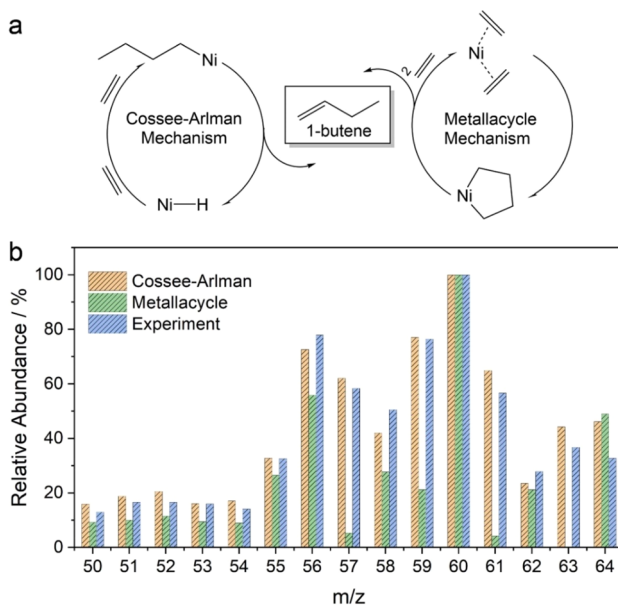


Figure 5. (a) Scheme of the two catalytic mechanisms for ethylene dimerization on a Ni center. (b) Experimental and theoretically predicted (based on the two mechanisms) fragmentation patterns of 1-butene produced from a mixture of $\text{C}_2\text{H}_4/\text{C}_2\text{D}_4$ (1:1).

coordinated to the active metal site to form metallacyclopentane, whereas the Cossee-Arlman mechanism is based on the successive insertion of ethylene.^{55,56} The two mechanisms can be distinguished by an isotope labeling experiment, using a 1:1 mixture of ethylene and perdeutero ethylene as the feeding gas.^{31,57} Theoretically, if the reaction proceeds via the Cossee-Arlman mechanism, the produced 1-butene isotopomers should consist of C_4H_8 , $\text{C}_4\text{H}_7\text{D}$, $\text{C}_4\text{H}_5\text{D}_3$, $\text{C}_4\text{H}_4\text{D}_4$, $\text{C}_4\text{H}_3\text{D}_5$, C_4HD_7 , and C_4D_8 in a 1:1:1:2:1:1 ratio. In contrast, if the reaction proceeds via the metallacycle mechanism, the product should consist of C_4H_8 , $\text{C}_4\text{H}_4\text{D}_4$, and C_4D_8 in a 1:2:1 ratio. This difference can be identified by analyzing the products with mass spectrometry. We used this established method to determine the reaction pathway of ethylene dimerization over Ni-ZIF-8 (Figures S14–S16 and Table S5). As indicated in Figure 5b, our experimental mass fragmentation pattern showed apparently better agreement with the pattern predicted by the Cossee-Arlman mechanism. The slight differences between the experimental values and the theoretical values may have been caused by H/D scrambling.

We performed density functional theory (DFT) calculations based on the Cossee-Arlman mechanism to evaluate the energetics of the catalytic reaction path on Ni-ZIF-8.⁵⁸ Given the easy departure of the NO_3^- and dangling imidazole groups upon the addition of MAO, the calculations start with the hydrogen-bonded Ni(II), which can easily catch an ethylene molecule to form the η -2 bond. The bonded ethylene is reoriented such that the carbon atom points toward the Ni-

bonded H and they form the ethyl group bonded to the Ni(II), leaving one empty site for the adsorption of another ethylene molecule. Then the chain prorogation reaction takes place to form a butyl group bonded to the Ni(II), followed by the formation of 1,2-butene through hydrogen rearrangement. Finally, a 1-butene molecule is formed with the breaking of the η -2 coordination bond. According to our calculations, the whole reaction path is smooth and energetically favorable (see Figures S17 and S18).

We attribute the high catalytic activity of Ni-ZIF-8 to the unique coordination environment of Ni. Unlike previously reported MOF-based catalysts that have Ni centers incorporated in the 3D framework or Ni complexes anchored on the walls of micropores, the Ni active sites of Ni-ZIF-8 were located on the crystal surface in a planar coordination geometry, with two imidazole ligands bonded to the MOF framework and two free ligands. Such a configuration is very similar to that of many molecular homogeneous catalysts. The steric effect has been documented to play a vital role in ethylene dimerization catalyzed by Ni-based homogeneous catalysts. Hence, we evaluated this effect and found that the Ni center in Ni-ZIF-8 had a 51.7% buried volume within a 5 Å radius spherical space (Figure S19), which is similar to the values of the four-coordinated molecular Ni catalyst^{59,60} and smaller than those of metal complexes with higher coordination numbers.⁶¹ Moreover, the two free ligands are loosely bonded to the Ni center and tend to leave during the reaction, providing sufficient space and vacant sites to facilitate ethylene adsorption and insertion. To further verify this hypothesis, we conducted ethylene dimerization under the standard reaction conditions using the core/shell-structured Ni-ZIF-8@ZIF-8 because, in Ni-ZIF-8@ZIF-8, the Ni centers were encapsulated within the crystal and presumably tetrahedrally coordinated with imidazoles in the 3D framework (unless local structural defects occur). In-line with our prediction, Ni was in an inactive state in this restricted environment, and the activity of Ni-ZIF-8@ZIF-8 was only about $1/7$ of the activity of Ni-ZIF-8 under the same conditions (TOF: 43 300 vs 297 000; entries 20 and 6 in Table 1). The limited activity of Ni-ZIF-8@ZIF-8 may have arisen from a small number of crystals that were not entirely coated and still had some surface Ni sites exposed.

CONCLUSION

In summary, we have demonstrated that, through a simple one-pot synthesis process, Ni^{2+} cations can be selectively anchored to the crystal surface of Ni-ZIF-8, where they adopt a planar four-coordinate configuration. These single sites of Ni are fully accessible to the reactant molecules without the mass-transport restrictions usually imposed by microporous supports. Their local structure is an analogue to homogeneous diimine Ni complexes. The asymmetric strengths of the coordination bonds in Ni-ZIF-8 retain Ni on the MOF crystal while providing vacant sites to promote the adsorption of reactant molecules during the reaction. Thus, Ni-ZIF-8 combines the advantages of heterogeneous and homogeneous catalysts and exhibits excellent stability and high catalytic activity in the ethylene dimerization reactions, thereby giving a significantly higher turnover number in a single reaction than most existing catalysts. These characteristics of Ni-ZIF-8 make it a suitable candidate catalyst for the continuous process of ethylene dimerization using fixed-bed or trickle-bed reactors. When the surface Ni atoms are incorporated into the 3D

MOF framework through a secondary growth process, they lose their catalytic activity, which confirms the close correlation between the catalytic activity and the unique position and coordination environment of the Ni centers. While this work focuses on the preparation of a highly active heterogeneous catalyst for ethylene dimerization, it should inspire the development of more MOF-based catalysts for other important reactions.

■ ASSOCIATED CONTENT

SI Supporting Information

The Supporting Information is available free of charge at <https://pubs.acs.org/doi/10.1021/jacs.1c02272>.

Experimental details for the syntheses and characterizations of materials, catalytic reactions, isotopic labeling experiments, and methods for theoretical calculations; Tables S1–S5; Figures S1–S19; Cartesian coordinates of the structure models ([PDF](#))

■ AUTHOR INFORMATION

Corresponding Author

Yu Han — Advanced Membranes and Porous Materials Center, Physical Sciences and Engineering Division, King Abdullah University of Science and Technology, Thuwal 23955-6900, Saudi Arabia;  orcid.org/0000-0003-1462-1118; Email: yu.han@kaust.edu.sa

Authors

Cailing Chen — Advanced Membranes and Porous Materials Center, Physical Sciences and Engineering Division, King Abdullah University of Science and Technology, Thuwal 23955-6900, Saudi Arabia;  orcid.org/0000-0003-2598-1354

Mohammed R. Alalouni — Advanced Membranes and Porous Materials Center, Physical Sciences and Engineering Division, King Abdullah University of Science and Technology, Thuwal 23955-6900, Saudi Arabia;  orcid.org/0000-0002-2945-3308

Xinglong Dong — Advanced Membranes and Porous Materials Center, Physical Sciences and Engineering Division, King Abdullah University of Science and Technology, Thuwal 23955-6900, Saudi Arabia

Zhen Cao — KAUST Catalysis Center, Physical Sciences and Engineering Division, King Abdullah University of Science and Technology, Thuwal 23955-6900, Saudi Arabia

Qingpeng Cheng — Advanced Membranes and Porous Materials Center, Physical Sciences and Engineering Division, King Abdullah University of Science and Technology, Thuwal 23955-6900, Saudi Arabia

Lirong Zheng — Beijing Synchrotron Radiation Facility, Institute of High Energy Physics, Chinese Academy of Sciences, Beijing 100049, P.R. China

Lingkun Meng — State Key Laboratory of Inorganic Synthesis and Preparative Chemistry, College of Chemistry, Jilin University, Changchun 130012, P.R. China

Chao Guan — KAUST Catalysis Center, Physical Sciences and Engineering Division, King Abdullah University of Science and Technology, Thuwal 23955-6900, Saudi Arabia

Lingmei Liu — Advanced Membranes and Porous Materials Center, Physical Sciences and Engineering Division, King Abdullah University of Science and Technology, Thuwal

23955-6900, Saudi Arabia;  orcid.org/0000-0002-3273-9884

Edy Abou-Hamad — Imaging and Characterization Core Lab, King Abdullah University of Science and Technology, Thuwal 23955-6900, Saudi Arabia

Jianjian Wang — Multi-scale Porous Materials Center, Institute of Advanced Interdisciplinary Studies, & School of Chemistry and Chemical Engineering, Chongqing University, Chongqing 400044, P.R. China;  orcid.org/0000-0002-9989-669X

Zhan Shi — State Key Laboratory of Inorganic Synthesis and Preparative Chemistry, College of Chemistry, Jilin University, Changchun 130012, P.R. China;  orcid.org/0000-0001-9717-1487

Kuo-Wei Huang — KAUST Catalysis Center, Physical Sciences and Engineering Division, King Abdullah University of Science and Technology, Thuwal 23955-6900, Saudi Arabia;  orcid.org/0000-0003-1900-2658

Luigi Cavallo — KAUST Catalysis Center, Physical Sciences and Engineering Division, King Abdullah University of Science and Technology, Thuwal 23955-6900, Saudi Arabia;  orcid.org/0000-0002-1398-338X

Complete contact information is available at:
<https://pubs.acs.org/10.1021/jacs.1c02272>

Author Contributions

▲C.C., M.R.A., and X.D. contributed equally to this work.

Notes

The authors declare no competing financial interest.

■ ACKNOWLEDGMENTS

The financial support for this work was provided by Baseline Funds (BAS/1/1372-01-01) to Y.H. from King Abdullah University of Science and Technology (KAUST). M.R.A would like to acknowledge Saudi Aramco Advanced Degree Program. This research used resources of the Core Laboratories of KAUST. The computational simulations were performed on the KAUST supercomputers.

■ REFERENCES

- (1) Bender, M. An Overview of Industrial Processes for the Production of Olefins - C₄ Hydrocarbons. *ChemBioEng Rev.* **2014**, *1*, 136–147.
- (2) Alenezi, H.; Alwi, S. R. W.; Manan, Z. A.; Zaidel, D. N. A. Recent Developments on Ethylene Dimerization with Focus on Alphabutol Optimization. *IJITEE* **2019**, *8*, 3969–3975.
- (3) Carter, C. O. Olefin dimerization. U.S. Patent, 4242531, July 2, 1980.
- (4) Al-Sherehy, F. A. IFP-SABIC process for the selective ethylene dimerization to butene-1. *Stud. Surf. Sci. Catal.* **1996**, *100*, 515–523.
- (5) Al-Sa'doun, A. W. Dimerization of ethylene to butene-1 catalyzed by Ti(OR')₄-AlR₃. *Appl. Catal., A* **1993**, *105*, 1–40.
- (6) Bryliakov, K. P.; Antonov, A. A. Recent progress of transition metal based catalysts for the selective dimerization of ethylene. *J. Organomet. Chem.* **2018**, *867*, 55–61.
- (7) Bianchini, C.; Giambastiani, G.; Luconi, L.; Meli, A. Olefin oligomerization, homopolymerization and copolymerization by late transition metals supported by (imino)pyridine ligands. *Coord. Chem. Rev.* **2010**, *254*, 431–455.
- (8) Wang, Z.; Liu, Q. B.; Solan, G. A.; Sun, W. H. Recent advances in Ni-mediated ethylene chain growth: N-imine-donor ligand effects on catalytic activity, thermal stability and oligo-/polymer structure. *Coord. Chem. Rev.* **2017**, *350*, 68–83.

- (9) Hulea, V. Toward platform chemicals from bio-based ethylene: heterogeneous catalysts and processes. *ACS Catal.* **2018**, *8*, 3263–3279.
- (10) Smith, P. D.; Klendworth, D. D.; Mcdaniel, M. P. Ethylene dimerization over supported titanium alkoxides. *J. Catal.* **1987**, *105*, 187–198.
- (11) Angelescu, E.; Che, M.; Andruh, M.; Zăvoianu, R.; Costentin, G.; Mirică, C.; Dumitru Pavel, O. Ethylene selective dimerization on polymer complex catalyst of $\text{Ni}(4,4'\text{-bipyridine})\text{Cl}_2$ coactivated with $\text{AlCl}(\text{C}_2\text{H}_5)_2$. *J. Mol. Catal. A: Chem.* **2004**, *219*, 13–19.
- (12) Lallemand, M.; Finiels, A.; Fajula, F.; Hulea, V. Ethylene oligomerization over Ni-containing mesostructured catalysts with MCM-41, MCM-48 and SBA-15 topologies. *Stud. Surf. Sci. Catal.* **2007**, *170*, 1863–1869.
- (13) Rossetto, E.; Nicola, B. P.; de Souza, R. F.; Bernardo-Gusmao, K.; Pergher, S. B. C. Heterogeneous complexes of nickel MCM-41 with beta-diimine ligands: Applications in olefin oligomerization. *J. Catal.* **2015**, *323*, 45–54.
- (14) Sohn, J. R.; Lee, S. Y. High catalytic activity of NiO-ZrO_2 modified with WO_3 for ethylene dimerization. *Appl. Catal., A* **1997**, *164*, 127–140.
- (15) McGuinness, D. S. Olefin oligomerization via metallacycles: dimerization, trimerization, tetramerization, and beyond. *Chem. Rev.* **2011**, *111*, 2321–41.
- (16) Canivet, J.; Aguado, S.; Schuurman, Y.; Farrusseng, D. MOF supported selective ethylene dimerization single site catalysts through one pot postsynthetic modification. *J. Am. Chem. Soc.* **2013**, *135*, 4195–4198.
- (17) Metzger, E. D.; Brozek, C. K.; Comito, R. J.; Dinca, M. Selective dimerization of ethylene to 1-butene with a porous catalyst. *ACS Cent. Sci.* **2016**, *2*, 148–161.
- (18) Metzger, E. D.; Comito, R. J.; Wu, Z. W.; Zhang, G. H.; Dubey, R. C.; Xu, W.; Miller, J. T.; Dinca, M. Highly selective heterogeneous ethylene dimerization with a scalable and chemically robust MOF catalyst. *ACS Sustainable Chem. Eng.* **2019**, *7*, 6654–6661.
- (19) Hu, Y.; Zhang, Y.; Han, Y.; Sheng, D.; Shan, D.; Liu, X.; Cheng, A. Ultrathin nickel-based metal-organic framework nanosheets as reusable heterogeneous catalyst for ethylene dimerization. *ACS Appl. Nano Mater.* **2019**, *2*, 136–142.
- (20) Wang, X. N.; Zhang, P.; Kirchon, A.; Li, J. L.; Chen, W. M.; Zhao, Y. M.; Li, B.; Zhou, H. C. Crystallographic visualization of postsynthetic nickel clusters into metal-organic framework. *J. Am. Chem. Soc.* **2019**, *141*, 13654–13663.
- (21) Yuan, S.; Zhang, P.; Zhang, L.; Garcia-Esparza, A. T.; Sokaras, D.; Qin, J. S.; Feng, L.; Day, G. S.; Chen, W.; Drake, H. F.; Elumalai, P.; Madrahimov, S. T.; Sun, D.; Zhou, H. C. Exposed equatorial positions of metal centers via sequential ligand elimination and installation in MOFs. *J. Am. Chem. Soc.* **2018**, *140*, 10814–10819.
- (22) Arrozi, U. S. F.; Bon, V.; Kutzscher, C.; Senkovska, I.; Kaskel, S. Towards highly active and stable nickel-based metal-organic frameworks as ethylene oligomerization catalysts. *Dalton Trans.* **2019**, *48*, 3415–3421.
- (23) Arrozi, U. S. F.; Bon, V.; Krause, S.; Lubken, T.; Weiss, M. S.; Senkovska, I.; Kaskel, S. In situ imine-based linker formation for the synthesis of zirconium MOFs: a route to CO_2 capture materials and ethylene oligomerization catalysts. *Inorg. Chem.* **2020**, *59*, 350–359.
- (24) Liu, B.; Jie, S.; Bu, Z.; Li, B.-G. Postsynthetic modification of mixed-linker metal-organic frameworks for ethylene oligomerization. *RSC Adv.* **2014**, *4*, 62343–62346.
- (25) Bernales, V.; League, A. B.; Li, Z.; Schweitzer, N. M.; Peters, A. W.; Carlson, R. K.; Hupp, J. T.; Cramer, C. J.; Farha, O. K.; Gagliardi, L. Computationally guided discovery of a catalytic cobalt-decorated metal-organic framework for ethylene dimerization. *J. Phys. Chem. C* **2016**, *120*, 23576–23583.
- (26) Ye, J. Y.; Gagliardi, L.; Cramer, C. J.; Truhlar, D. G. Computational screening of MOF-supported transition metal catalysts for activity and selectivity in ethylene dimerization. *J. Catal.* **2018**, *360*, 160–167.
- (27) Liu, J.; Ye, J. Y.; Li, Z. Y.; Otake, K.; Liao, Y. J.; Peters, A. W.; Noh, H.; Truhlar, D. G.; Gagliardi, L.; Cramer, C. J.; Farha, O. K.; Hupp, J. T. Beyond the active site: tuning the activity and selectivity of a metal-organic framework-supported Ni catalyst for ethylene dimerization. *J. Am. Chem. Soc.* **2018**, *140*, 11174–11178.
- (28) Agirrezabal-Telleria, I.; Luz, I.; Ortuno, M. A.; Oregui-Bengoechea, M.; Gandarias, I.; Lopez, N.; Lail, M. A.; Soukri, M. Gas reactions under intrapore condensation regime within tailored metal-organic framework catalysts. *Nat. Commun.* **2019**, *10*, 2076.
- (29) Madrahimov, S. T.; Gallagher, J. R.; Zhang, G. H.; Meinhart, Z.; Garibay, S. J.; Delferro, M.; Miller, J. T.; Farha, O. K.; Hupp, J. T.; Nguyen, S. T. Gas-phase dimerization of ethylene under mild conditions catalyzed by MOF materials containing (bpy) Ni^{II} complexes. *ACS Catal.* **2015**, *5*, 6713–6718.
- (30) Li, Z.; Schweitzer, N. M.; League, A. B.; Bernales, V.; Peters, A. W.; Getsoian, A.; Wang, T. C.; Miller, J. T.; Vjunov, A.; Fulton, J. L.; Lercher, J. A.; Cramer, C. J.; Gagliardi, L.; Hupp, J. T.; Farha, O. K. Sintering-resistant single-site nickel catalyst supported by metal organic framework. *J. Am. Chem. Soc.* **2016**, *138*, 1977–1982.
- (31) Metzger, E. D.; Comito, R. J.; Hendon, C. H.; Dinca, M. Mechanism of single-site molecule-like catalytic ethylene dimerization in Ni-MFU-4I. *J. Am. Chem. Soc.* **2017**, *139*, 757–762.
- (32) Comito, R. J.; Metzger, E. D.; Wu, Z.; Zhang, G.; Hendon, C. H.; Miller, J. T.; Dinca, M. Selective dimerization of propylene with Ni-MFU-4I. *Organometallics* **2017**, *36*, 1681–1683.
- (33) Antonov, A. A.; Semikolenova, N. V.; Talsi, E. P.; Matsko, M. A.; Zakharov, V. A.; Bryliakov, K. P. 2-iminopyridine nickel(II) complexes bearing electron-withdrawing groups in the ligand core: Synthesis, characterization, ethylene oligo- and polymerization behavior. *J. Organomet. Chem.* **2016**, *822*, 241–249.
- (34) Zubkevich, S. V.; Tuskaev, V. A.; Gagieva, S. C.; Pavlov, A. A.; Khrustalev, V. N.; Zarubin, D. N.; Kurmaev, D. A.; Kolosov, N. A.; Bulychev, B. M. Molecular structure, magnetic properties and catalytic activity in selective ethylene dimerization of nickel (II) complexes with bis(3,5-dimethylpyrazol-1-yl)methane. *J. Mol. Struct.* **2020**, *1206*, 127692.
- (35) Tayade, K. N.; Mane, M. V.; Sen, S.; Murthy, C. N.; Tembe, G. L.; Pillai, S. M.; Vanka, K.; Mukherjee, S. A catalytic and DFT study of selective ethylene oligomerization by nickel(II) oxime-based complexes. *J. Mol. Catal. A: Chem.* **2013**, *366*, 238–246.
- (36) Olivier-Bourbigou, H.; Breuil, P. A. R.; Magna, L.; Michel, T.; Espada Pastor, M. F.; Delcroix, D. Nickel catalyzed olefin oligomerization and dimerization. *Chem. Rev.* **2020**, *120*, 7919–7983.
- (37) Koshy, D.; Chen, S.; Lee, D. U.; Burke Stevens, M.; Abdellah, A.; Dull, S.; Chen, G.; Nordlund, D.; Gallo, A.; Hahn, C.; Higgins, D. C.; Bao, Z.; Jaramillo, T. Understanding the origin of highly selective CO_2 electroreduction to CO on Ni, N-doped carbon catalysts. *Angew. Chem., Int. Ed.* **2020**, *59*, 4043–4050.
- (38) Fei, H.; Dong, J.; Feng, Y.; Allen, C. S.; Wan, C.; Voloskiy, B.; Li, M.; Zhao, Z.; Wang, Y.; Sun, H.; An, P.; Chen, W.; Guo, Z.; Lee, C.; Chen, D.; Shakir, I.; Liu, M.; Hu, T.; Li, Y.; Kirkland, A. I.; Duan, X.; Huang, Y. General synthesis and definitive structural identification of Mn_4C_4 single-atom catalysts with tunable electrocatalytic activities. *Nat. Catal.* **2018**, *1*, 63–72.
- (39) Zhao, C. M.; Dai, X. Y.; Yao, T.; Chen, W. X.; Wang, X. Q.; Wang, J.; Yang, J.; Wei, S. Q.; Wu, Y. E.; Li, Y. D. Ionic exchange of metal organic frameworks to access single nickel sites for efficient electroreduction of CO_2 . *J. Am. Chem. Soc.* **2017**, *139*, 8078–8081.
- (40) Wu, Y.; Yuan, D.; He, D.; Xing, J.; Zeng, S.; Xu, S.; Xu, Y.; Liu, Z. Decorated traditional zeolites with subunits of metal-organic frameworks for CH_4/N_2 separation. *Angew. Chem., Int. Ed.* **2019**, *58*, 10241–10244.
- (41) Damyanova, S.; Pawelec, B.; Palcheva, R.; Karakirova, Y.; Sanchez, M. C. C.; Tyuliev, G.; Gaigneaux, E.; Pierro, J. L. G. Structure and surface properties of ceria-modified Ni-based catalysts for hydrogen production. *Appl. Catal., B* **2018**, *225*, 340–353.
- (42) Zubkevich, S. V.; Tuskaev, V. A.; Gagieva, S. C.; Kayda, A. S.; Khrustalev, V. N.; Pavlov, A. A.; Zarubin, D. N.; Bulychev, B. M. NNNO-Heteroscorpionate nickel (II) and cobalt (II) complexes for

- ethylene oligomerization: the unprecedented formation of odd carbon number olefins. *Appl. Organomet. Chem.* **2020**, *34*, No. e5873.
- (43) Antonov, A. A.; Semikolenova, N. V.; Soshnikov, I. E.; Talsi, E. P.; Bryliakov, K. P. Selective ethylene dimerization into 2-butene using homogeneous and supported nickel(II) 2-iminopyridine catalysts. *Top. Catal.* **2020**, *63*, 222–228.
- (44) Wei, W.; Yu, B. W.; Alam, F.; Huang, Y. W.; Cheng, S. L.; Jiang, T. Ethylene oligomerization promoted by nickel-based catalysts with silicon-bridged diphosphine amine ligands. *Transition Met. Chem.* **2019**, *44*, 125–133.
- (45) Huang, Y.; Zhang, L.; Wei, W.; Alam, F.; Jiang, T. Nickel-based ethylene oligomerization catalysts supported by PNSiP ligands. *Phosphorus, Sulfur Silicon Relat. Elem.* **2018**, *193*, 363–368.
- (46) Rozhko, E.; Bavykina, A.; Osadchii, D.; Makkee, M.; Gascon, J. Covalent organic frameworks as supports for a molecular Ni based ethylene oligomerization catalyst for the synthesis of long chain olefins. *J. Catal.* **2017**, *345*, 270–280.
- (47) Pinheiro, A. C.; Virgili, A. H.; Roisnel, T.; Kirillov, E.; Carpentier, J. F.; Casagrande, O. L. Ni(II) complexes bearing pyrrolide-imine ligands with pendant N-, O- and S-donor groups: synthesis, structural characterization and use in ethylene oligomerization. *RSC Adv.* **2015**, *5*, 91524–91531.
- (48) Boulens, P.; Pellier, E.; Jeanneau, E.; Reek, J. N. H.; Olivier-Bourbigou, H.; Breuil, P.-A. R. Self-assembled organometallic nickel complexes as catalysts for selective dimerization of ethylene into 1-butene. *Organometallics* **2015**, *34*, 1139–1142.
- (49) Ulbrich, A. H. D. P. S.; Campedelli, R. R.; Milani, J. L. S.; dos Santos, J. H. Z.; Casagrande, O. D. Nickel catalysts based on phenyl ether-pyrazol ligands: Synthesis, XPS study, and use in ethylene oligomerization. *Appl. Catal., A* **2013**, *453*, 280–286.
- (50) Chandran, D.; Byeon, S. J.; Suh, H.; Kim, I. Effect of ion-pair strength on ethylene oligomerization by divalent nickel complexes. *Catal. Lett.* **2013**, *143*, 717–722.
- (51) Boudier, A.; Breuil, P.-A. R.; Magna, L.; Olivier-Bourbigou, H.; Braunstein, P. Nickel(II) complexes with imino-imidazole chelating ligands bearing pendant donor groups (SR, OR, NR₂, PR₂) as precatalysts in ethylene oligomerization. *J. Organomet. Chem.* **2012**, *718*, 31–37.
- (52) Mukherjee, S.; Patel, B. A.; Bhaduri, S. Selective ethylene oligomerization with nickel oxime complexes. *Organometallics* **2009**, *28*, 3074–3078.
- (53) Buchard, A.; Auffrant, A.; Klemps, C.; Vu-Do, L.; Boubeker, L.; Le Goff, X. F.; Le Floch, P. Highly efficient P-N nickel(II) complexes for the dimerisation of ethylene. *Chem. Commun.* **2007**, 1502–1504.
- (54) Lejeune, M.; Semeril, D.; Jeunesse, C.; Matt, D.; Peruch, F.; Lutz, P. L.; Ricard, L. Diphosphines with expandable bite angles: Highly active ethylene dimerisation catalysts based on upper rim, distally diphosphinated calix[4]arenes. *Chem. - Eur. J.* **2004**, *10*, 5354–5360.
- (55) Grubbs, R. H.; Miyashita, A. Metallacyclopentanes as catalysts for the linear and cyclodimerization of olefins. *J. Am. Chem. Soc.* **1978**, *100*, 7416–7418.
- (56) Cossee, P. Ziegler-Natta catalysis I. Mechanism of polymerization of α -olefins with Ziegler-Natta catalysts. *J. Catal.* **1964**, *3*, 80–88.
- (57) Suttil, J. A.; McGuinness, D. S. Mechanism of ethylene dimerization catalyzed by Ti(OR')₄/AlR₃. *Organometallics* **2012**, *31*, 7004–7010.
- (58) Deng, L. Q.; Margl, P.; Ziegler, T. A density functional study of Nickel(II) diimide catalyzed polymerization of ethylene. *J. Am. Chem. Soc.* **1997**, *119*, 1094–1100.
- (59) Falivene, L.; Wiedemann, T.; Gottker-Schnetmann, I.; Caporaso, L.; Cavallo, L.; Mecking, S. Control of chain walking by weak neighboring group interactions in unsymmetrical catalysts. *J. Am. Chem. Soc.* **2018**, *140*, 1305–1312.
- (60) Schiebel, E.; Santacroce, S.; Falivene, L.; Gottker-Schnetmann, I.; Caporaso, L.; Mecking, S. Tailored strength neighboring group interactions switch polymerization to dimerization catalysis. *ACS Catal.* **2019**, *9*, 3888–3894.
- (61) Falivene, L.; Cao, Z.; Petta, A.; Serra, L.; Poater, A.; Oliva, R.; Scarano, V.; Cavallo, L. Towards the online computer-aided design of catalytic pockets. *Nat. Chem.* **2019**, *11*, 872–879.